Available online at www.sciencedirect.com
SCIENCE DIRECT®
Acta Materialia 53 (2005) 4163–4171
Acta MATERIALIA
www.actamat-journals.com

Effects of temperature, strain rate and grain size on the compressive properties of Ti_3SiC_2

T. Zhen, M.W. Barsoum *, S.R. Kalidindi

Department of Materials Science and Engineering, Drexel University, Philadelphia, PA 19104, United States

Received 11 February 2005; accepted 3 May 2005
Available online 11 July 2005

Abstract

Herein we report on the response of polycrystalline Ti_3SiC_2 samples, with two grain sizes, on cyclic compressive loading in the 25–1200 °C temperature range. At lower temperatures, the stress–strain curves outline fully reversible, closed loops whose size and shape depend on grain size, but not strain rate. This phenomenon is attributed to the formation and annihilation of incipient kink bands, defined to be thin plates of sheared material bounded by opposite walls of dislocations that as long as the dislocation walls remain attached, are attracted to each other and annihilate upon removal of the load. Because the dislocations are confined to the basal planes, dislocation forests do not form and the dislocations can move reversibly over relatively large distances dissipating a significant (25% at 1 GPa) portion of the mechanical energy. At high temperatures (>1000 °C), the stress–strain loops are open, the response is strain rate dependent and cyclic hardening is observed for both microstructures. In this regime, kink bands and dislocation arrays interact in such a way as to form deformation cells that are smaller than the original grains and that, in turn, leads to hardening.

Keywords: Ti_3SiC_2; Compression; High temperature; Kink bands

1. Introduction

Recently, the ternary carbides and nitrides with the general formula $M_{n+1}AX_n$, where $n = 1$ to 3, M is an early transition metal, A is an A-group (mostly IIIA and IVA) element and X is C and/or N, have been the subject of intense research, especially by this group [1,2]. There are roughly 50 M_2AX phases [4]; three M_3AX_2 (Ti_3SiC_2 [5], Ti_3AlC_2 [6] and Ti_3GeC_2 [7]) and one M_4AX_3 viz. Ti_4AlN_3 [8,3]. The vast majority of these phases were discovered and synthesized in powder form by Nowotny and co-workers in the 1960s [4]. Renewed interest in these phases was triggered when it was established that these solids exhibit unusual, and sometime unique, combinations of properties [9]. Like metals, they are electrically and thermally conductive, exceptionally thermal shock resistant and damage tolerant [1,2,9–27]. Their hardness values fall in the narrow range of 3–6 GPa (i.e., harder than most metals, but softer than most ceramics). Like ceramics, some are elastically rigid and lightweight. One of their more surprising but characteristic properties is their machinability; they are machinable, using nothing more sophisticated than a manual hack saw, or regular high-speed tool steels.

By far the best characterized of these compounds is Ti_3SiC_2. Its electric and thermal conductivities are twice those of pure Ti [9,10]. Its thermoelectric power is negligible over the 4–850 K temperature range [12], which led to the conclusion that it is a compensated conductor, in which the concentration and mobilities of electrons are equal to those of holes [12]. With a Young's modulus of 340 GPa [9,13,14] and a density

* Corresponding author. Tel.: +1 215 895 6760.
E-mail address: barsoumw@drexel.edu (M.W. Barsoum).

1359-6454/$30.00
doi:10.1016/j.actamat.2005.05.020

of 4.5 gm/cm^3, its specific stiffness is almost three times that of Ti, a metal prized for its high specific stiffness. It is also refractory (dissociation temperature of >2300 °C [15]), fatigue [16], creep [17,18] and oxidation resistant up to 900 °C [20]. It has a brittle-to-plastic transition, BPT, at 1100 °C [17–19]. At 0.5, the strain rate sensitivity is exceptionally high for a crystalline, non-superplastic material [18]. This high strain sensitivity is exhibited by both fine (3–5 μm), and coarse (100–200 μm) grained samples [18]. Its fracture toughness exhibits *R*-curve behavior with initial toughness values of 8–10 MPa$\sqrt{}$m, that can rise to 16 MPa$\sqrt{}$m, depending on crack extension and grain size [16].

Most of the mechanical properties of the MAX phases, including the ones described herein, can be traced to the following three facts:

(i) Basal slip, and only basal slip, is operative at all temperatures. The Burgers vector in the basal plane is 3.01 Å; any non-basal dislocation would have to have a Burgers vector >17 Å [21,22]. They thus lack the five independent slip systems required for ductility. If the grains are oriented and large, Ti_3SiC_2 is ductile at room temperature [23].
(ii) Because of their high *c*/*a* ratios, twinning is unlikely, and has never been observed. Instead, these compounds deform by the formation of kink bands, KBs, within individual grains [21–25].
(iii) Because they are confined to the basal planes, the dislocations arrange themselves either in arrays (pile-ups) on the same slip plane, or in walls (viz. low or high angle grain boundaries) normal to the arrays [21,22]. The only interactions possible are those where the arrays and walls intersect. This does not allow for the formation of forests of dislocations, for example, and concomitant work hardening in the classic sense. Hence, dislocations can move back and forth reversibly and extensively, resulting in a new physical phenomenon in crystalline solids, best described as fully reversible dislocation-based deformation (see below) [1].

Li et al. [26] were the first to report on the non-linear response of Ti_3SiC_2 in bending at room temperature; an observation they ascribed to a combination of microcracking and deformation. The effect was small and the hysteresis loops obtained were open. Radovic et al. [18] cycled fine-grained Ti_3SiC_2 in tension and were the first to report closed hysteresis loops in the narrow stress range between 120 and 200 MPa.

More recently, it has been shown that macroscopic polycrystalline Ti_3SiC_2 cylinders of varying grain sizes can be compressed at room temperature to stresses of up to 1 GPa and fully recover upon the removal of the load [1]. The stress–strain curves at room temperature are non-linear, outline fully reversible reproducible closed loops whose size and shape depend on grain size, but not strain rate. The energy dissipated per cycle, W_d, for Ti_3SiC_2 is higher than most woods, and comparable to polypropylene and nylon. Furthermore, W_d was found to roughly scale with the square of the applied stress, σ.

This phenomenon was attributed to the formation and annihilation of fully reversible incipient kink bands (IKBs) [1,27–29,32,33], defined to be thin plates of sheared material bounded by near parallel dislocation walls of opposite polarity that remain attached, and are thus attracted to each other. Removal of the load allows the walls to collapse and the total elimination of the IKB. At temperatures >1000 °C, the stress–strain loops are open and the response becomes strain-rate dependent [1]. Cyclic hardening however, is observed at 1200 °C, for both fine and coarse-grained samples [1]. Apparently at higher temperatures the IKBs dissociate into parallel mobile dislocation walls, that in turn coalesce to form regular KBs that are no longer reversible [1].

The purpose of this paper is to report on the compressive behavior of Ti_3SiC_2 both at room and elevated temperatures. The results of a compressive creep study at high temperatures will be published elsewhere [30].

2. Experimental procedure

The processing details can be found elsewhere [31]. Briefly, stoichiometric powder mixtures of titanium (−325 mesh, 99.5%, Alfa Aesar, Ward Hill, MA), silicon carbide (−400 mesh, 99.5%, Atlantic Engineering Equipment, Bergenfield, NJ) and graphite (−300 mesh, 99%, Alfa Aesar, Ward Hill, MA) were reactively hot isostatically pressed (HIPed). HIPing at 1450 °C under a pressure of 40 MPa for 4 h resulted in a fine-grained (FG) microstructure; HIPing at 1600 °C at a pressure of 40 MPa for 6 h resulted in a coarse-grained (CG) microstructure. Details of the microstructural characterization can be found elsewhere [19].

Compression tests were performed on cylindrically shaped specimens (9.8 mm in diameter and 30 mm high), that were electro-discharge machined and tested with no further surface preparation. All the tests were performed in air using a hydraulic testing machine (MTS 810), equipped with a controller (Microconsoler 458.20) that allowed tests to be run in displacement or load control mode. In all tests, a ~2 MPa preload was applied to keep the sample aligned. Strains were measured by a high-temperature capacitance MTS extensometer, with 5% capacity; the force was measured using a load cell with 100 kN capacity. The gauge length was 25 mm.

3. Results

3.1. Room temperature response

When FG Ti_3SiC_2 cylinders were compressed cyclically with progressively higher stresses up to a maximum stress of 1 GPa all loading curves were quite similar (Fig. 1). As important, and despite the fact that the deformation was fully reversible up to 1 GPa, the response was non-linear. The time dependencies of the stresses and strains recorded during cycling twice to 1 GPa were identical showing excellent reproducibility and reversibility [1].

The full reversibility of the deformation was also not a function of the number of cycles, at least up to 100 cycles. When a FG Ti_3SiC_2 sample was cycled 100 times to 718 MPa (inset Fig. 2), apart from a small permanent deformation and a slight hardening, the differences between the first and the last stress–strain loops were small (Figs. 2). The same was true for a CG sample cycled 100 times at 250 MPa [34].

To investigate strain rate effects, two different tests were carried out on the different microstructures. When the stress–strain results from three load/unload cycles at strain rates of 10^{-5}, 10^{-4} and 10^{-3} s^{-1} were plotted on the same curve (Fig. 3) it is clear that the response is independent of strain rate in the range explored. The reproducibility of the loops is noteworthy. To further explore this important aspect, a FG sample was loaded to 600 MPa; unloaded to 450 MPa, held at that stress for one minute before further unloading to 250 MPa and held there for another minute. The corresponding dependencies of strain and stress on time clearly show the samples do *not* creep at room temperature at 450 MPa (Fig. 4). Note also that there is only one unloading trajectory (inset Fig. 4).

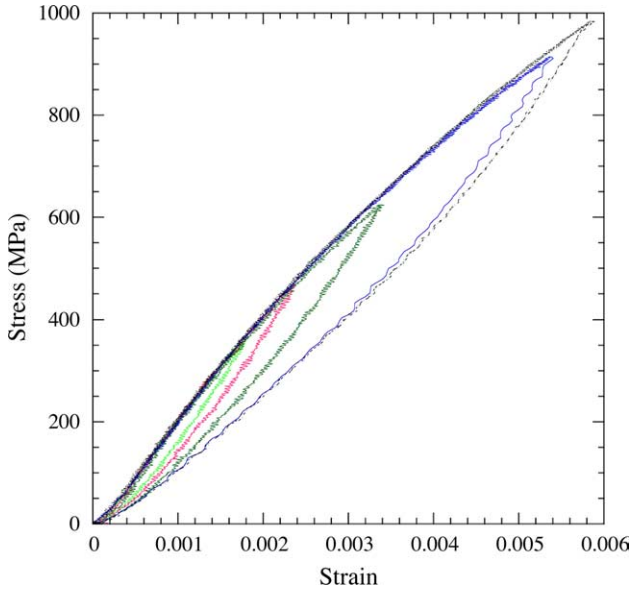

Fig. 1. (a) Room temperature loading–unloading stress–strain curves for FG Ti_3SiC_2 to successively higher stresses. Note presence of one loading curve.

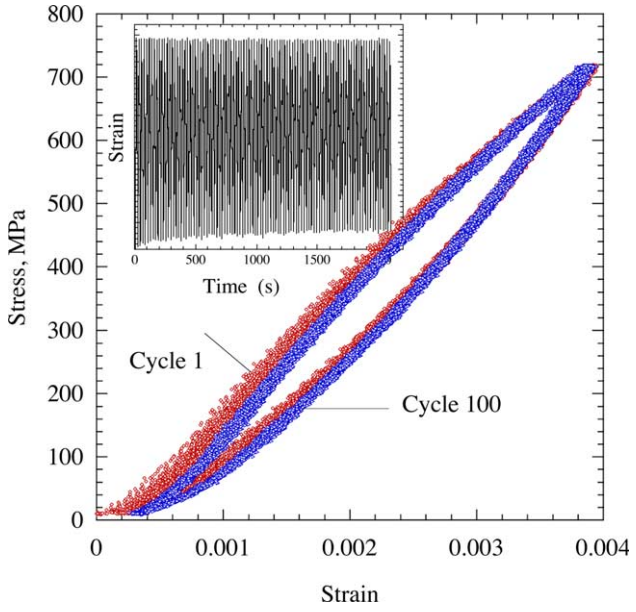

Fig. 2. Room temperature cyclic loading–unloading stress–strain curves for FG Ti_3SiC_2 cylinders loaded to 700 MPa 100 times. The 100 cycles are plotted. Inset shows strain variations versus time. Note reproducibility.

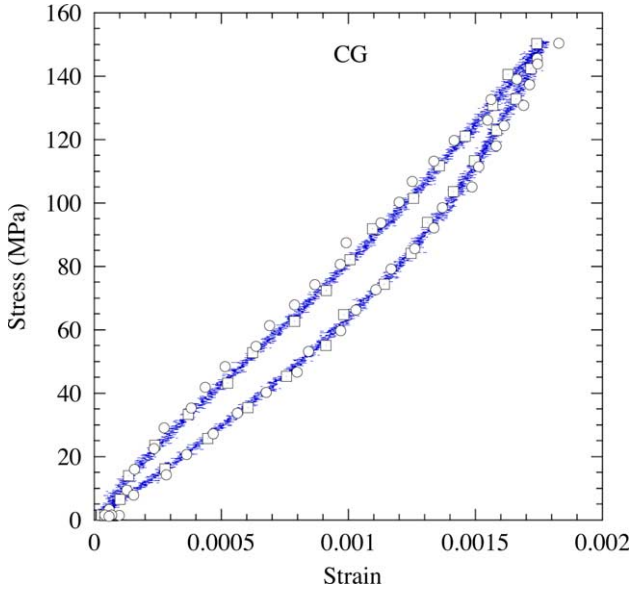

Fig. 3. Room temperature stress–strain curves of a CG Ti_3SiC_2 sample loaded to 160 MPa at three strain rates varying by an order of magnitude each (see text). In the strain rate regime tested, and with the resolution of our extensometer, the cycles appear to be indistinguishable.

3.2. Effect of temperature

Typical loading–unloading stress–strain curves for CG and FG Ti_3SiC_2 cylinders loaded in compression

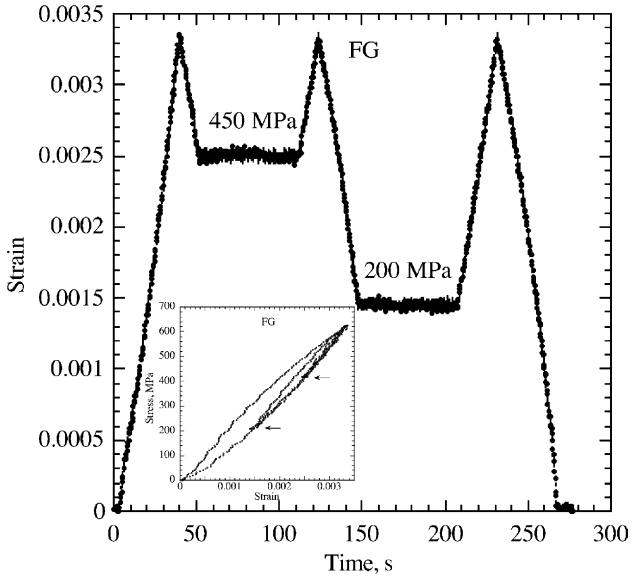

Fig. 4. Strain versus time curves for FG sample loaded to 600 MPa, unloaded to 450 and 200 MPa and held at each stress level for 1 min, before reloading to 600 MPa. Clearly, the sample does not creep. Inset shows the corresponding stress–strain curves. Note presence of one unloading curve.

to 160 MPa at different temperatures are shown in Figs. 5(a) and (b), respectively. The stress/strain curves for both microstructures at 1200 °C are compared in the inset of Fig. 5(b). Fig. 5(c) plots the stress and strain time dependencies at 1200 °C. Similarly, Fig. 5(d) plots the time dependencies for a similar experiment, except that now the unloading rates were 10 times slower. These results clearly establish that:

(i) Both microstructures become softer with increasing temperatures, with the effect being more pronounced for the CG microstructure (inset Fig. 5(b)).
(ii) The initial slopes of the stress–strain cycles are close to the true elastic modulus (as determined from ultrasound measurements [14,32]) of the FG samples at lower temperatures (Fig. 5(b)), but start to deviate from the RT response at increasingly lower stress levels as the temperature is increased.
(iii) The response of the CG samples at 500 °C (Fig. 5(a)) is comparable to that of the FG samples at 1100 °C (Fig. 5(b)). Up to 140 MPa, the response of the latter is linear elastic up to 900 °C (Fig. 5(b)).
(iv) At 1100 °C for the CG samples, and at 1200 °C for both microstructures, the hysteretic loops are open and the response is time dependent.
(v) Both the relaxation times and total recovered strain are higher in the CG microstructure than its FG counterpart (Fig. 5(c)). The differences in the responses of the FG and CG microstructures are more pronounced if the unloading rates are fast (Fig. 5(c)), than if they are slow (Fig. 5(d)). The slower unloading rates result in distinct bow outs in the corresponding stress/strain curves (see Ref. [1, Fig. 3a]). These bow outs reflect the fact that the strain maxima do not coincide with the stress maxima (Fig. 5(d)). In other words, the samples keep shrinking for a relatively long time after the load is removed.

3.3. Cyclic hardening at 1200 °C

Fig. 6(a) plots 21 stress/strain cycles for a CG sample at 1200 °C. When the color-coded cycles shown in Fig. 6(a) are re-plotted such that they all start from zero strain (Fig. 6(b)) the effect of cycling is unambiguous. Cyclic hardening is manifested by both a reduction in the total areas enclosed by the successive cycles and a general stiffening. Note that it is only *after* the sample is cycled a few times that a clearly defined elastic response at low strains is observed. By the 21st cycle, the slope on loading is ~270 GPa (solid straight line in Fig. 6(b)), and thus comparable to the value of Young's modulus as determined from ultrasound measurements at that temperature, viz. 288 GPa [32].

Fig. 7 compares the *room temperature* compressive loading–unloading stress–strain curves of a CG sample *before* and *after* a 2% deformation at 100 MPa at 1300 °C. Here again, the 1300 °C deformation resulted in hardening. As importantly, the first cycle after the high temperature test is open and encloses a larger area than the second – and subsequent cycles (not shown) – that trace fully reversible or closed loops.

The dissipated energy per cycle, W_d, and its temperature and microstructure dependence was published elsewhere (Ref. [1, Fig. 4]) and will not be repeated here.

4. Discussion

The results presented herein confirm and further enhance our understanding of kinking non-linear elastic (KNE) solids in general, and the MAX phases in particular. Because the response at lower temperatures is fully reversible and rate-independent, while that at higher temperatures is not, each will be dealt with separately below.

4.1. Fully reversible regime

The response of KNE solids in this regime has been discussed thoroughly in a number of previous papers [1,27–29,33] and is reasonably well understood. In short, the application of a load initially results in the formation of dislocation pile-ups (DPs) in "soft" grains viz. those

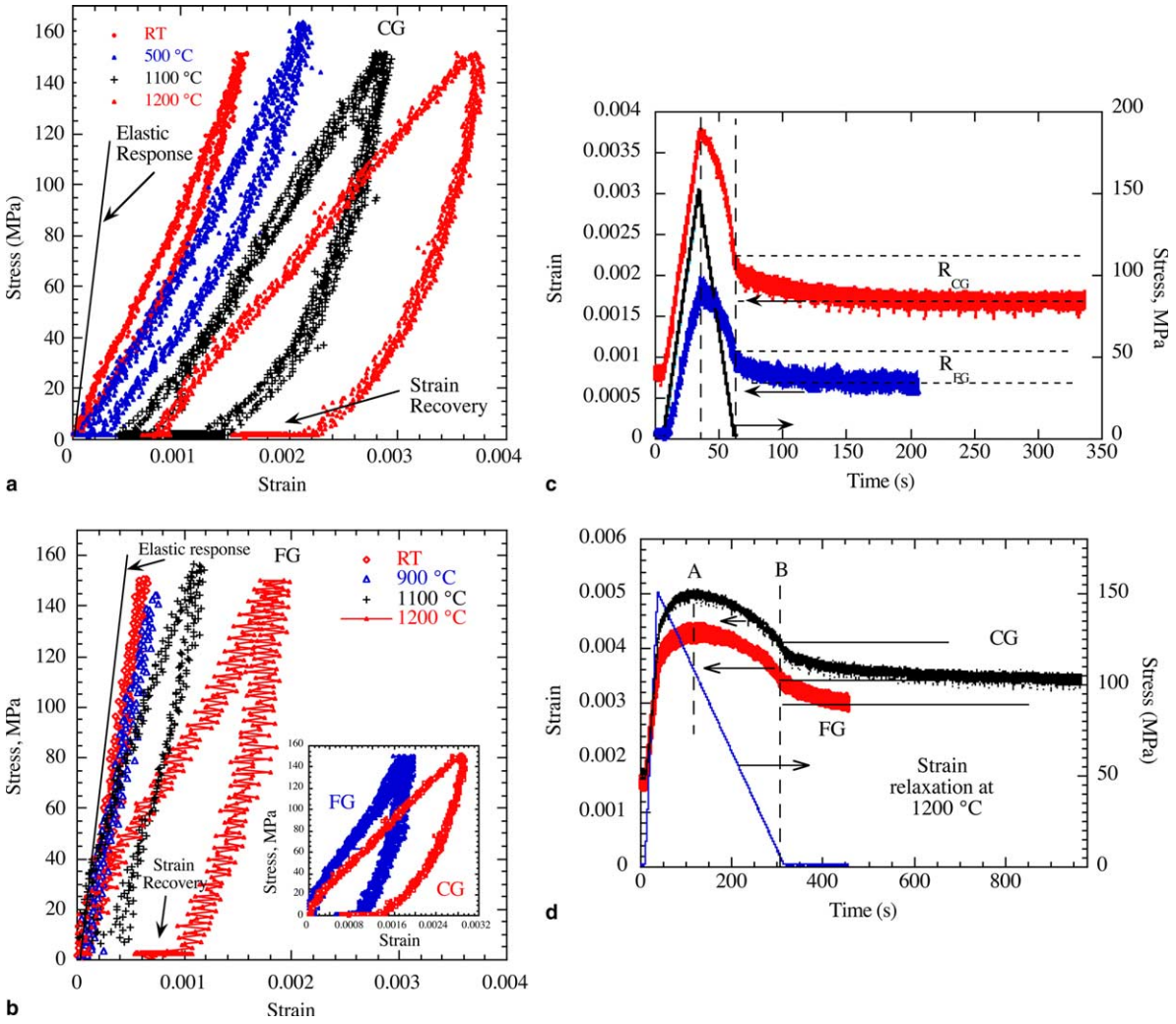

Fig. 5. Temperature dependence of cyclic stress–strain curves for: (a) CG and (b) FG Ti_3SiC_2 samples. Inset in b compares the first cycles for both microstructures. Time dependencies of stress and strain during loading and unloading of both microstructures, at 1200 °C, for (c) relatively fast unloading, and (d) slower unloading. In (c) and (d), the strain axis is on the left and the stress axis is on the right. Note time delay in the position of the maximum stress and maximum strain. Also note relaxation after load is removed.

favorably oriented to the applied load [33]. At higher stresses, fully reversible IKBs form in the "hard" grains. In the FG material, the IKB density is $\approx 10^{18}$ m^{-3} [33]. What the results of this work add is further evidence for the reversibility of the process (Fig. 1(a)), its insensitivity to strain rate (Fig. 3) – at least in the 10^{-5}–10^{-3} s^{-1} range – and, as important, the robustness of the material to cycling (Fig. 2). It is worth noting that the slight hardening observed on cycling (Fig. 2) rules out microcracking as a source of the hysteresis. It also augers well for the fatigue resistance of this material and is consistent with the excellent fatigue properties reported [35]. Lastly, Fig. 4 clearly shows that at room temperature, the FG material does not creep, even at stresses of ≈450 MPa.

The lack of five independent slip systems ensures that some of the pile-up stress will be borne by the grain boundaries. As for most materials, the CG samples are weaker than the FG ones. It has been previously shown that CG samples of Ti_3SiC_2 emitted an acoustic signal before failure; FG samples, on the other hand, were silent [36]. This difference was attributed to microcracking as a result of pile-ups, a conclusion that this work shows is probably incomplete, since delaminations (see below) are probably also occurring. However, the fact that the FG material can withstand 1 GPa indicates that the grain boundaries in these materials are fairly strong.

At temperatures lower than the brittle-to-plastic transition, BPT, temperature of Ti_3SiC_2 (1100–1200 °C) [17–19], the hysteretic loops are almost fully closed or reversible. That is true of the CG samples at 500 and 900 °C (Fig. 5(a)), and the FG samples at 1100 °C (Fig. 5(b)). This reversibility is consistent with a situation where we are dealing with IKBs almost exclusively.

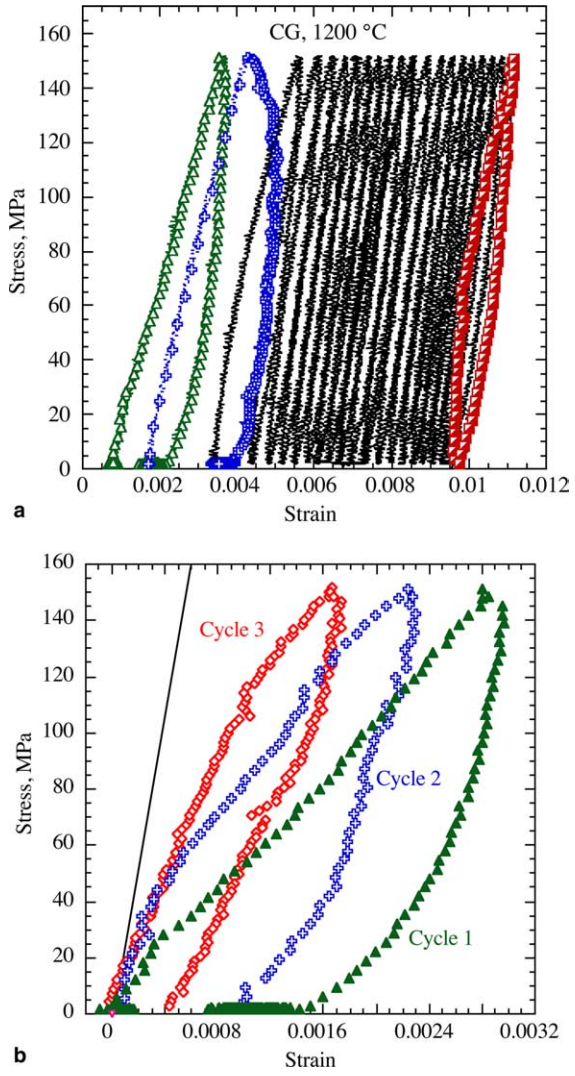

Fig. 6. Compressive cyclic loading of a CG cylinder at 1200 °C. (a) totality of cycles; (b) comparison of cycles 1, 2 and 21, in (a). In (b) all cycles start at the origin. Cyclic hardening is unambiguous. Solid inclined line represents a Young's modulus of $E = 270$ GPa, which is the expected linear elastic response at that temperature based on ultrasound measurements.

At 1100 °C for the CG samples, and at 1200 °C in both microstructures, the loops are clearly larger and open (Figs. 5(a) and (b)) and the response is time dependent (Figs. 5(c) and (d)) indicating, as discussed in the next section, that in addition to IKBs we now have mobile dislocation walls, MDWs, and dislocation pile-ups, DPs, to contend with.

4.2. Partially reversible regime

This and previous work [1] leave little doubt that stress cycling, even at temperatures as high as 1200 °C, results in hardening (Fig. 6). Simple high temperature deformation also results in hardening after cooling to room temperature (Fig. 7). According to Frank and Stroh (F&S) [37], and our modifications of their theory

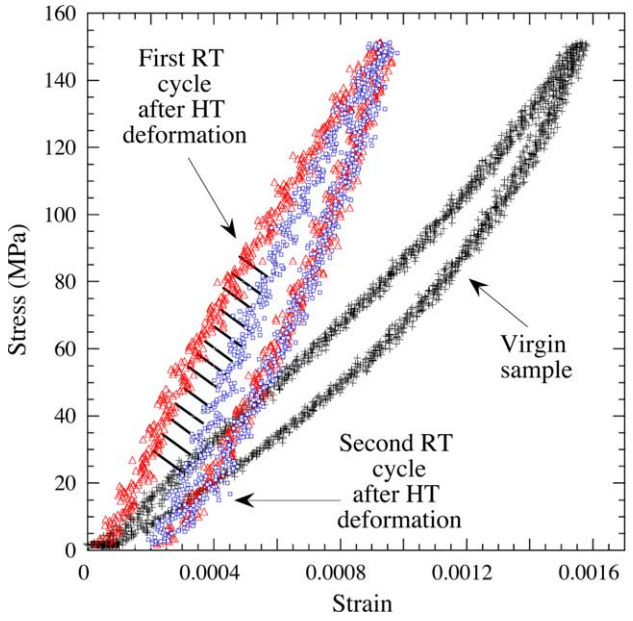

Fig. 7. Effect of 2% deformation (1300 °C and 100 MPa), on room temperature cyclic stress–strain curves of a CG sample. After the high temperature deformation the response is more like that of a FG material than a CG sample. Note that first cycle after deformation is slightly open, but the next, and all subsequent (not shown) cycles are identical and fully reversible.

[33], the remote shear stress needed to initiate an IKB is given by:

$$\tau > \tau_c \geqslant \sqrt{\frac{G^2 b \gamma_c}{2\alpha_c}}, \tag{1}$$

where G is the shear modulus, b the Burgers vector, γ_c the critical angle of kinking, which for most solids is of the order of 5°; $2\alpha_c$ is the width of a grain (i.e., thickness of grain along the c-direction). This equation is fundamental to understanding the deformation of KNE solids in general, and the hardening observed herein in particular. Based on Eq. (1), a reduction in α should result in hardening.

Further, the results shown in Fig. 7 provide indirect, but compelling, evidence for the formation of MDWs at elevated temperatures and their annihilation at room temperature. Based on the discussion so far, it is not unreasonable to assume that during the 1300 °C deformation, the following elements are present in the microstructure: DPs, MDWs, and KBs. During unloading and cooling, the DPs should relax (see below), but the MDWs and KBs will presumably be unaffected. Upon reloading, again at room temperature, the preexisting MDWs are swept into the KBs resulting in the small permanent deformation observed during the first cycle. Upon reloading a second time, only IKBs are nucleated and the response not only becomes fully reversible once again, but as important, is now much more characteristic of a FG microstructure than the original CG one.

This latter observation provides the strongest evidence for the hypothesis that the high temperature deformation resulted in a reduction of the effective grain size.

In Ti_3SiC_2, the energy expended in forming DPs is roughly two orders of magnitude lower than that expended in forming IKBs [33]. This in turn implies that the areas under the stress–strain curves shown in Figs. 5(a) and (b), 6 and 7, are largely due to the formation of IKBs, MDWs and KBs, and not DPs. The formation of MDWs and KBs is in general expected to be accompanied by delamination. However, the hardening observed during cycling at temperature (Fig. 6) and after a moderate amount of plastic (irreversible) deformation at 1300 °C (Fig. 7) indicates that there must be a regime of high temperature plastic deformation that can occur in these materials without significant delamination. During such plastic deformation, the grains are expected to breakdown into smaller grains resulting in the observed hardening. It is clear that this regime of high temperature plastic deformation without significant delamination is somewhat restricted in extent, because at higher levels of plastic deformation there is evidence of delamination and microcracking along with the breakup of large grains into smaller ones, as seen in Fig. 8.

There is about a 500 °C reduction in the temperature at which the hysteretic loops open for the CG relative to the FG material (compare Figs. 5(a) and (b)). This suggests that the transition from IKBs to MDWs and KBs occurs more readily in the CG material compared to the FG material. Although the precise reasons for this observation are not yet completely clear, the analysis by Stroh [38] offers some insight. By considering the initiation of a crack at the end of a low angle tilt boundary of length 2α, he showed that cleavage along the basal planes would occur when:

$$\sigma_n\sigma_s \geqslant \frac{k\gamma G}{2\alpha\pi}, \tag{2}$$

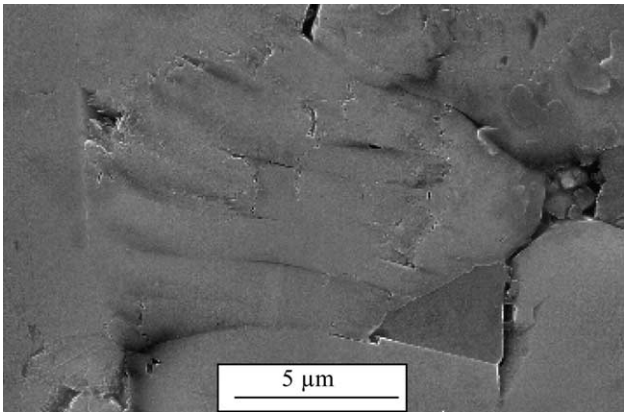

Fig. 8. SEM micrograph of a sample deformed at high temperatures, showing the break-up of a large grain into smaller rectangular-like domains.

where σ_n is the applied stress; σ_s the resolved shear stress on the basal planes; γ the surface energy of the cleavage planes; k is a numerical constant that depends on the elastic anisotropy of the crystal. In a polycrystal, according to Eq. (2), all else being equal, thicker grains (i.e., those with the largest α's) should delaminate first. Since delamination is the critical event for the transition of IKBs to MDWs and KBs, this transition will occur at lower stresses, and by extension at lower temperatures, in the CG material than the FG material, as observed.

Lastly, we need to address the strong time dependence of the response at temperatures above the brittle-to-plastic transition, BPT, temperature. In this regime, there are large residual internal stresses operative long after the stress is removed (e.g. Figs. 5(c) and (d)). To understand these differences, one must invoke or appreciate the interplay of DPs, with grain boundaries, GBs. The stress concentration due to a DP is given by [39]:

$$\sigma_x = C_0\left(\frac{\lambda}{x}\right)^{1/2}, \tag{3}$$

where C_0 is a constant and x is the distance from the tip. The pile-up length is typically assumed to scale with grain size. For hexagonal grains that tend to grow into thin disks, λ is the diameter of the disk (i.e., the dimension along [1 0 0]).

At higher temperatures, it is reasonable to assume the GBs are softer, and consequently, the IKBs can now detach and create MDWs, which in turn result in plastic deformation and ultimately KBs. The softening can also allow the DPs to run into the GBs, causing the latter and/or triple points to slide and cavitate. Direct microstructural evidence for the latter mechanism has been shown previously (e.g., Ref. [19, Fig. 9]).

As in our previous work [17–19], we take the recovery upon unloading (Figs. 5(c) and (d)) to be unambiguous evidence for the presence of large internal stresses. The facts that both the characteristic relaxation times (Fig. 5(c)) and the absolute recovery of the CG samples are greater than those of the FG samples (compare R_{CG} to R_{FG} in Fig. 5(c)) after identical loading conditions imply that the internal stress is also dependent on the microstructure; the larger the grain size, the larger the internal stresses, a conclusion totally consistent with the notion that these stresses are due to DPs.

Perhaps the single most compelling evidence that DPs *and* delaminations play a crucial role in the deformation of Ti_3SiC_2 is the *reduction* in fracture toughness, K_{1c}, at temperatures greater than the BPT temperature [24]. This fact is primarily why we do not refer to the BPT by its more common moniker, the ductile-to-brittle transformation or DBT temperature, because it clearly does not signify the activation of new slip systems. As

important, the results of this work shed some light on what occurs at temperatures > BPT. In deriving Eq. (2), Stroh did not consider the presence of DPs normal to the low angle tilt boundary. In TEM analyses of KBs and DPs in Ti_3SiC_2 it was noted that delamination tended to occur on the basal planes in which the DPs had formed, thus eliminating them [22], further reducing the strain energy of the system. In as much as the DPs placed back-pressure on an advancing crack increasing K_{1c}, their elimination should result in a lower K_{1c}. The results shown herein, especially the SEM micrograph shown in Fig. 8, are consistent with such a notion. Also consistent with this interpretation are the profuse amounts of microcracks and cavities observed near the main cracks of compact tension specimens tested at 1200 °C for both microstructures (see Ref. [24, Figs. 7 and 8]).

It is important to note that in this regime, cycling to the same stress leads to the establishment of an equilibrium microstructure in which only IKBs are active, as exemplified by the last loops shown in Fig. 6(a). It is also important to note that Ti_3SiC_2, and presumably the other MAX phases, are very resistant to dynamic recrystallization. In one case a 30-kg Vickers indentation was introduced in a Ti_3SiC_2 sample prior to annealing it for 48 h at 1600 °C. After annealing, the morphology of the sample in the near vicinity of the indentation was identical to that before annealing. It would thus appear that the strain energies associated with the rectangular cells formed upon loading (e.g., Fig. 8) are insufficient to cause recrystallization even under extreme annealing conditions.

5. Conclusions

Based on this and previous work, four regimes for the mechanical response of Ti_3SiC_2, and by extension the other 50 + MAX phases, have been identified:

(i) If remote applied shear stress, τ, is less than the right-hand side, RHS, in Eq. (1), the response is elastic as exemplified by the FG samples at temperatures <1100 °C (Fig. 5(b)). The response is also elastic if stress cycling, or simple deformation reduces the domain size, 2α, to an extent that $\tau <$ RHS of Eq. (1). This is exemplified by the emergence of a purely elastic regime in the CG samples at low stresses with cycling (Fig. 6(b)). The same occurs in the FG microstructure; the effect is more pronounced, however (see Ref. [1, Fig. 3(b)]).

(ii) A regime in which τ is less than the RHS of Eq. (1), but the product $\sigma_n\sigma_s$ is <RHS of Eq. (2). In that case, fully reversible, hysteric loops form even at stresses of the order of 1 GPa [1]. The response depends on microstructure, not strain rate. This is attributed to the formation and annihilation of IKBs that are fully reversible.

(iii) A regime in which both inequalities in Eqs. (1) and (2) are exceeded. In that case, the first loop is slightly open, but all subsequent cycles to the same stress result in fully reversible closed hysteric loops. In this regime, the stress is high enough to cause delaminations and transition of IKBs to MDWs and KBs. Under certain circumstances, especially for small amounts of plastic (irreversible) strains at high temperatures, the main consequence appears to be a reduction of effective grain size in the material resulting in hardening as per Eq. (1).

(iv) At the highest temperatures, the KBs, MDWs and DPs play a major role and the response becomes time dependent. Once in this regime, the response is a strong function of strain rate. Cycling to the same stress, however, leads to the establishment of an equilibrium microstructure in which only IKBs are active.

Acknowledgement

This work was funded by the Army Research Office (DAAD19-03-1-0213).

References

[1] Barsoum MW, Zhen T, Kalidindi S, Radovic M, Murugaiah A. Fully reversible dislocation-based deformation of Ti_3SiC_2 to 1 GPa. Nat Mater 2003;2:107–11.

[2] Barsoum MW. The $M_{n+1}AX_n$ phases: A New Class of solids: thermodynamically stable nanolaminates. Prog Sol State Chem 2000;28:201–81.

[3] Nowotny H. Struktuchemie Einiger Verbindungen der Ubergangsmetalle mit denelementen C, Si, Ge, Sn. Prog Solid State Chem 1970;27.

[4] Jeitschkl W, Nowotny H. Die Kristallstructur von Ti_3SiC_2 – Ein Neuer Komplxcarbid-Typ. Monatsh Chem 1967;98:329–37.

[5] Pietzka MA, Schuster JC. Summary of constitution data of the system Al–C–Ti. J Phase Equilib 1994;15:392.

[6] Wolfsgruber H, Nowotny H, Benesovsky F. Die Kristallstuktur von Ti_3GeC_2. Monatsh Chem 1967;9:2401.

[7] Barsoum MW, Farber L, Levin I, Procopio A, El-Raghy T, Berner A. HRTEM of Ti_4AlN_3; or $Ti_3Al_2N_2$ Revisited. J Am Ceram Soc 1999;82:2545–7.

[8] Rawn CJ, Barsoum MW, El-Raghy T, Procopio A, Hoffmann CM, Hubbard C. Structure of Ti_4AlN_{3-x}- a Layered $M_{n+1}AX_n$ nitride. Mater Res Bull 2000;35:1785.

[9] Barsoum MW, El-Raghy T. Synthesis and characterization of a remarkable ceramic: Ti_3SiC_2. J Amer Cer Soc 1996;79:1953–6.

[10] Barsoum MW, El-Raghy T, Rawn CJ, Porter WD, Wang H, Payzant A, et al. Thermal properties of Ti_3SiC_2. J Phys Chem Solids 1999;60:429.

[11] Yoo H-I, Barsoum MW, El-Raghy T. Ti_3SiC_2 has negligible thermopower. Nature 2000;407:581–2.
[12] Finkel P, Hettinger J, Lofland S, Barsoum MW, El-Raghy T. Hall effect, magnetoresistance and magnetic susceptibility of Ti_3SiC_2 in the 4–300 K range. Phys Rev B 2002;65:35113.
[13] Pampuch R, Lis J, Stobierski L, Tymkiewicz M. Solid combustion synthesis of Ti_3SiC_2. J Eur Ceram Soc 1989;5:283.
[14] Finkel P, Barsoum MW, El-Raghy T. Low temperature dependencies of the elastic properties of $Ti_3Al_{1.1}C_{1.8}$, Ti_4AlN_3 & Ti_3SiC_2. J Appl Phys 2000;87:1701–3.
[15] Du Y, Schuster JC, Seifert H, Aldinger F. Experimental investigation and thermodynamic calculation of the Titanium–Silicon–Carbon system. J Am Ceram Soc 2000;83:197–203.
[16] Gilbert CJ, Bloyer DR, Barsoum MW, El-Raghy T, Tomsia AP, Ritchie RO. Fatigue-crack growth and fracture properties of coarse and fine-grained Ti_3SiC_2. Scripta Mater 2000;42:761–7.
[17] Radovic M, Barsoum MW, El-Raghy T, Wiederhorn S. Tensile creep of fine-grained (3–5 μm) Ti_3SiC_2 in the 1000–1200 °C temperature range. Acta Mater 2001;49:4103–12.
[18] Radovic M, Barsoum MW, El-Raghy T, Wiederhorn S, Luecke W. Effect of temperature, strain rate and grain size on the mechanical response of Ti_3SiC_2 in tension. Acta Mater 2002;50:1297–306.
[19] Radovic M, Barsoum MW, El-Raghy T, Wiederhorn S. Tensile creep of coarse-grained (100–300 μm) Ti_3SiC_2 in the 1000–1200 °C temperature range. J Alloys Compd 2003;361:299–312.
[20] Barsoum MW, Ho-Duc LH, Radovic M, El-Raghy T. Long time oxidation study of Ti_3SiC_2, Ti_3SiC_2/SiC and Ti_3SiC_2/TiC composites in air. J Electrochem Soc 2003;150:B166–75.
[21] Farber L, Levin I, Barsoum MW. HRTEM study of a low-angle boundary in plastically deformed Ti_3SiC_2. Philos Mag Lett 1999;79:163.
[22] Barsoum MW, Farber L, El-Raghy Dislocations T. Kink banks and room temperature plasticity of Ti_3SiC_2. Metall Mater Trans 1999;30A:1727–38.
[23] Barsoum MW, El-Raghy T. Room temperature ductile carbides. Metall Mater Trans 1999;30A:363–9.
[24] Chen D, Shirato K, Barsoum MW, El-Raghy T, Ritchie RO. High-temperature cyclic fatigue-crack growth in monolithic Ti_3SiC_2 ceramics. J Am Ceram Soc 2001;84:2914.
[25] El-Raghy T, Barsoum MW, Zavaliangos A, Kalidindi SR. Processing and mechanical properties of Ti_3SiC_2: II, effect of grain size and deformation temperature. J Am Ceram Soc 2001;84:2855–60.
[26] Li J–F, Pan W, Sato F, Watanabe R. Mechanical properties of polycrystalline Ti_3SiC_2 at ambient and elevated temperatures. Acta Mater 2001;49:937.
[27] Murugaiah A, Barsoum MW, Kalidindi SR, Zhen T. Spherical nanoindentations in Ti_3SiC_2. J Mater Res 2004;19:1139–48.
[28] Barsoum MW, Murugaiah A, Kalidindi SR, Zhen T. Kinking nonlinear elastic solids, nanoindentations and geology. Phys Rev Lett 2004;92:255508-1.
[29] Barsoum MW, Murugaiah A, Kalidindi SR, Gogotsi Y. Kink bands, nonlinear elasticity and nanoindentations in graphite. Carbon 2004;42:1435–45.
[30] Zhen T, Barsoum MW, Kalidindi SR. Compressive Creep of Ti_3SiC_2 in the 1100 to 1300 °C temperature range in air. Acta Mater (in press).
[31] El-Raghy T, Barsoum MW. Processing and mechanical properties of Ti_3SiC_2: Part I: reaction path and microstructure evolution. J Am Ceram Soc 1999;82:2849–54.
[32] Barsoum MW, Radovic M, Zhen T, Finkel P. Dynamic elastic hysteretic solids and dislocations. Phys Rev Lett 2005;94:085501.
[33] Barsoum MW, Zhen T, Zhou A, Basu S, Kalidindi SR. Microscale modeling of kinking nonlinear elastic solids. Phys Rev B 2005;71:134101.
[34] Zhen T. PhD Thesis, Drexel University, June 2004.
[35] Zhang H, Wang ZG, Zang QS, Zhang ZF, Sun ZM. Cyclic fatigue crack propagation behavior of Ti_3SiC_2 synthesized by pulse discharge sintering (PDS) technique. Scripta Mater 2003;49:87–92.
[36] Barsoum MW, Radovic M, Finkel P, El-Raghy T. Ti_3SiC_2 and ice. Appl Phys Lett 2001;79:479–81.
[37] Frank FC, Stroh AN. On the theory of kinking. Proc Phys Soc 1952;65:811.
[38] Stroh AN. The cleavage of metal single crystals. Philos Mag 1958;3:597–606.
[39] Dowling NE. Mechanical behavior of metals. 2nd ed. Upper Saddle River (NJ): Prentice-Hall; 1998.